AGU PUBLICATIONS

Global Biogeochemical Cycles

RESEARCH ARTICLE
10.1002/2016GB005578

Key Points:
- Carbonate buffering is a major control on CO_2 oversaturation in streams and rivers
- Continuous CO_2 oversaturation can occur due to diel cycles of production and respiration, especially in high-alkalinity waters
- Landscape-scale patterns of CO_2 and DIC are differentiated between high- and low-alkalinity waters due to carbonate buffering

Supporting Information:
- Supporting Information S1

Correspondence to:
E. G. Stets,
estets@usgs.gov

Citation:
Stets, E. G., D. Butman, C. P. McDonald, S. M. Stackpoole, M. D. DeGrandpre, and R. G. Striegl (2017), Carbonate buffering and metabolic controls on carbon dioxide in rivers, *Global Biogeochem. Cycles*, *31*, 663–677, doi:10.1002/2016GB005578.

Received 7 NOV 2016
Accepted 15 MAR 2017
Accepted article online 20 MAR 2017
Published online 11 APR 2017

Carbonate buffering and metabolic controls on carbon dioxide in rivers

Edward G. Stets[1], David Butman[2], Cory P. McDonald[3], Sarah M. Stackpoole[4], Michael D. DeGrandpre[5], and Robert G. Striegl[1]

[1]U.S. Geological Survey National Research Program, Boulder, Colorado, USA, [2]School of Environmental and Forest Sciences, University of Washington, Seattle, Washington, USA, [3]Superior Hydroscience, Marquette, Michigan, USA, [4]U.S. Geological Survey National Research Program, Denver, Colorado, USA, [5]Department of Chemistry and Biochemistry, University of Montana, Missoula, Montana, USA

Abstract Multiple processes support the significant efflux of carbon dioxide (CO_2) from rivers and streams. Attribution of CO_2 oversaturation will lead to better quantification of the freshwater carbon cycle and provide insights into the net cycling of nutrients and pollutants. CO_2 production is closely related to O_2 consumption because of the metabolic linkage of these gases. However, this relationship can be weakened due to dissolved inorganic carbon inputs from groundwater, carbonate buffering, calcification, and anaerobic metabolism. CO_2 and O_2 concentrations and other water quality parameters were analyzed in two data sets: a synoptic field study and nationwide water quality monitoring data. CO_2 and O_2 concentrations were strongly negatively correlated in both data sets ($\rho = -0.67$ and $\rho = -0.63$, respectively), although the correlations were weaker in high-alkalinity environments. In nearly all samples, the molar oversaturation of CO_2 was a larger magnitude than molar O_2 undersaturation. We used a dynamically coupled O_2–CO_2 model to show that lags in CO_2 air-water equilibration are a likely cause of this phenomenon. Lags in CO_2 equilibration also impart landscape-scale differences in the behavior of CO_2 between high- and low-alkalinity watersheds. Although the concept of carbonate buffering and how it creates lags in CO_2 equilibration with the atmosphere is well understood, it has not been sufficiently integrated into our understanding of CO_2 dynamics in freshwaters. We argue that the consideration of carbonate equilibria and its effects on CO_2 dynamics are primary steps in understanding the sources and magnitude of CO_2 oversaturation in rivers and streams.

Plain Language Summary Carbon dioxide (CO_2) emission from streams and rivers is known to be large. The source of CO_2 in these systems is of high interest to researchers because it provides important clues about the carbon cycle and the overall biogeochemical functioning of freshwaters. The scientific questions surrounding CO_2 emissions from freshwaters have focused on whether CO_2 is produced within the aquatic environment through the decomposition of organic material or whether CO_2 is produced mostly in soil and groundwater and then delivered to freshwater environments where it is passively emitted to the atmosphere. Both explanations have a basis in reality, and yet neither fully explains the magnitude of estimated CO_2 emissions. We examined how CO_2 interacts with the rest of the carbonate buffering system to structure CO_2 emission to the atmosphere. We found that daily cycles in photosynthesis and decomposition can create continuous CO_2 oversaturation because of lags created through carbonate buffering. At the landscape scale, differences were evident in CO_2 excess between watersheds having high versus low carbonate buffering. Our conclusions highlight that carbonate buffering is the primary control on CO_2 concentration in surface waters and needs to be considered to understand the observations of CO_2 excess in freshwaters.

1. Introduction

Carbon dioxide (CO_2) supersaturation is widespread in inland waters [*Butman and Raymond*, 2011; *Kempe*, 1982]. Proper attribution of the processes leading to nearly ubiquitous CO_2 excess in streams has important implications for interpretation of stream metabolism, the aquatic carbon cycle, and the net cycling of nutrients and other pollutants. For example, in situ production of CO_2 through net heterotrophy suggests that surface waters are highly mineralizing environments with rapid turnover of nutrients and pollutants. On the other hand, CO_2 oversaturation maintained primarily through inputs of groundwater suggests that processes occurring in the terrestrial environment or in subsurface systems may be major controls on the carbon cycle in surface waters. A better process-level understanding of carbon cycling in streams is also important to improving estimation and reducing the uncertainty in aquatic carbon fluxes.

CO_2 is produced by multiple processes that can vary in space and time, making it difficult to generalize about its sources to surface waters. Input of allochthonous organic material and its subsequent oxidation in surface waters has been a major focus of aquatic carbon cycling [*Battin et al*., 2008; *Lapierre et al*., 2013; *McCallister and Del Giorgio*, 2012]. CO_2 oversaturation has also been attributed to groundwater inputs [*Finlay*, 2003; *Humborg et al*., 2010; *Oquist et al*., 2009], organic matter mineralization in riparian or hyporheic areas [*Baker et al*., 1999; *Laudon et al*., 2011; *Schindler and Krabbenhoft*, 1998], and cycles of calcite precipitation [*Tobias and Böhlke*, 2011]. All of these processes contribute to the maintenance of CO_2 oversaturation in surface waters and its significant efflux from stream surfaces.

The stoichiometry of CO_2 and O_2 in aquatic systems is of particular interest because of the insight it provides into the processes maintaining CO_2 oversaturation and how this relates to the interaction of stream metabolism and carbon biogeochemistry more broadly. CO_2 and O_2 concentrations are often strongly negatively correlated in inland surface waters [*Borges et al*., 2015; *Crawford et al*., 2014] because production of CO_2 from the oxidation of organic matter is coupled, directly or indirectly, to O_2 depletion through aerobic respiration, photo-oxidation, and chemical oxygen demand. CO_2 oversaturation in excess of O_2 depletion, including simultaneous CO_2 and O_2 oversaturation, is commonly observed [*McDonald et al*., 2013]. CO_2 oversaturation that greatly exceeds O_2 undersaturation seemingly contradicts the direct aerobic metabolic control of CO_2 dynamics in freshwater ecosystems and points toward additional mechanisms for CO_2 oversaturation. Various processes that would decouple CO_2 production from O_2 consumption have been invoked to explain this phenomenon. They include inputs of strong acids (for example, from acid deposition or acid mine drainage), which would titrate HCO_3^- to CO_2 without consuming O_2 [*Abril et al*., 2000]; anaerobic respiration, which produces dissolved inorganic carbon (DIC) without consuming oxygen [*Richey et al*., 1988; *Salomão et al*., 2008]; respiration occurring in rooted macrophytes [*Hamilton et al*., 1995]; calcite precipitation [*Marce et al*., 2015]; or inputs of high DIC groundwater [*Hotchkiss et al*., 2015].

Deviations from the expected stoichiometry of CO_2 and O_2 have also been attributed to lags in CO_2 equilibration created by interactions between CO_2 and the carbonate buffering system [*DeGrandpre et al*., 1998; *Parker et al*., 2005]. Although this effect has been known for several decades [see, for example, *Sundquist et al*., 1979], it has received far less attention in freshwater systems. And while oceanic systems contain a relatively constrained range of carbonate buffering strength, freshwaters span large ranges in alkalinity, pH, and CO_2 concentrations. This creates spatial and temporal differences in the strength of carbonate buffering, but much less is known about this aspect of freshwater carbon cycling.

Interpretation of CO_2:O_2 stoichiometry requires consideration of biological controls as well as the dynamics of the carbonate buffering system. CO_2 and O_2 have different solubilities in water and so are expected to have different concentrations at atmospheric equilibrium. Aerobic metabolism couples the production and consumption of O_2 and CO_2 such that the molar departures of the gases from atmospheric equilibrium, ΔO_2 and ΔCO_2, respectively, are expected to have predictable behavior. However, in water with relatively high pH (~8.0 or higher), the hydrated form of CO_2, H_2CO_3, can ionize to $H^+ + HCO_3^-$ [*Butler*, 1982], and so ΔCO_2 and $-\Delta O_2$ will be neither equivalent nor related by a fixed stoichiometry. In high-pH/high-alkalinity waters, some of the CO_2 added or removed through reactions such as primary production and aerobic respiration will exist in the ionized form. The CO_2 gradient across the air-water interface is also affected by ionization reactions and causes lags in CO_2 dynamics relative to O_2 [*DeGrandpre et al*., 1998].

We compared the molar deviations of O_2, CO_2, and DIC from atmospheric saturation in two complementary data sets spanning small headwater reaches to large rivers. Field synoptic and long-term water quality monitoring data were analyzed and cover a broad range of temporal and spatial scales. Water quality monitoring data have been used in previous studies to scale CO_2 concentration and flux estimates [*Butman and Raymond*, 2011]; however, CO_2 observations rely upon calculations by using pH, alkalinity, and temperature, which can be biased [*Abril et al*., 2015], and small headwater streams are often underrepresented. A combined analysis using water quality monitoring data along with field observations of CO_2 using in situ probes was used in order to strengthen the overall interpretability of the findings. CO_2:O_2 stoichiometry was analyzed in the context of the carbonate buffering system to provide greater detail on the processes maintaining CO_2 oversaturation in streams and rivers. We also present model results of coupled O_2 and CO_2 equilibria that demonstrate that interactions with the carbonate buffering system affect the

stoichiometry of ΔO_2 and ΔCO_2 and lead to landscape-scale differences in the behavior of CO_2 in high- versus low-alkalinity systems.

2. Methods

2.1. Study Approach

The field data set is from a synoptic survey of 101 streams distributed across the United States [*Stets et al.*, 2015], and the water quality monitoring data were obtained from the U.S. Geological Survey (USGS) National Water Information System (https://doi.org/10.5066/F7P55KJN) at 339 sites around the conterminous U.S. The data sets demonstrate the behavior of CO_2 and O_2 at different scales and using complementary methodology. Analyzing the data sets together strengthens the overall conclusions of the study. Throughout the manuscript, we refer to aqueous $CO_2 + H_2CO_3$ (i.e. H_2CO_3*) as CO_2.

2.2. Synoptic Field Survey

The field survey data consist of single samples from >100 stream sites distributed throughout the conterminous USA [*Stets et al.*, 2015] (Figure 1). The surveys included small streams in the mid-Atlantic and Southeastern USA, coastal rivers in the Pacific Northwestern USA, and sites tributary to the Upper Mississippi River in Minnesota and Wisconsin, USA. Sites spanned first-order streams to major tributaries and main stem sites on the Mississippi River that have annual average discharge $>200\ m^3\ s^{-1}$. At each site we recorded basic field information and collected water quality samples. Sampling occurred during summer and autumn in 2012–2014.

Basic field data were collected by using multiparameter sondes. In the Southeastern USA, a Yellow Springs Instruments 6920V2 sonde was used (Yellow Springs, OH, USA), and an EXO2 sonde (www.exowater.com) was used in the Pacific Northwest, USA, and Upper Mississippi sampling locations. Optical dissolved oxygen (DO) and pH probes (glass electrode) were calibrated at least once every 3 days during the field campaigns. DO was calibrated by using the saturated air technique, while pH probes were calibrated by using National Institute of Standards and Technology standards. In the field, sondes were allowed to equilibrate for at least 20 min before reading. Manufacturer specifications list the accuracy of optical DO probes as $\pm 0.01\ mg\ L^{-1}$ and pH probes as ±0.01 pH units.

For all field observations, pCO_2 was obtained by using a hand-held Vaisala Carbocap CO_2 meter [*Johnson et al.*, 2010]. During sampling the Vaisala probe was positioned just under the stream surface and allowed to equilibrate for >20 min. Pressure and temperature readings from a sonde were used to correct CO_2 readings per manufacturer's instructions. Statistical comparisons between the Vaisala meter and a more rigorous syringe equilibration technique [*Striegl and Michmerhuizen*, 1998] showed a strongly linear relationship with a slope near 1 (probe CO_2 ($\mu mol\ L^{-1}$) = [4.6 ± 4.7] + [0.92 ± 0.03] × syringe CO_2 ($\mu mol\ L^{-1}$), $R^2 = 0.95$, $P < 0.001$, $n = 78$; Figure S1 in the supporting information). In wadeable streams, discharge and stream velocity were measured at the time of sampling [*Rantz et al.*, 1982], while in larger rivers, real-time discharge estimates from USGS streamgages were used [*Stets et al.*, 2015].

Water was also collected for laboratory analysis of dissolved organic carbon (DOC), major ions, and alkalinity. At each sampling location, stream water was filtered through a 0.45 μm capsule filter by using a peristaltic pump (Geotech, Inc.). The capsule filters were flushed with at least 1 L of sample water prior to sample collection. Filtered water was kept cool and dark, shipped to the USGS office in Boulder, CO, and analyzed within 7 days of collection. DOC concentration was determined via platinum catalyzed persulfate wet oxidation on an Ocean Instruments Analytical Model 700 TOC analyzer (Ocean Instruments, Inc., San Diego, CA, USA). Alkalinity was measured by inflection-point titration using an autotitrator (Mettler Toledo). Major anions were measured by ion chromatography using a Dionex DX-120 ion chromatograph fitted with an IonPac AS14 column (Dionex Corporation, Sunnyvale, CA, USA). Cations were measured by using a Perkin Elmer 3300DV inductively coupled plasma optical emission spectrometer in the axial viewing configuration. All elements were calibrated by using 5- or 6-point calibration curves.

2.3. Water Quality Monitoring Data

Relationships between CO_2, O_2, and other water quality parameters were also tested by using USGS databases. The water quality monitoring data originated from USGS monitoring networks and were obtained

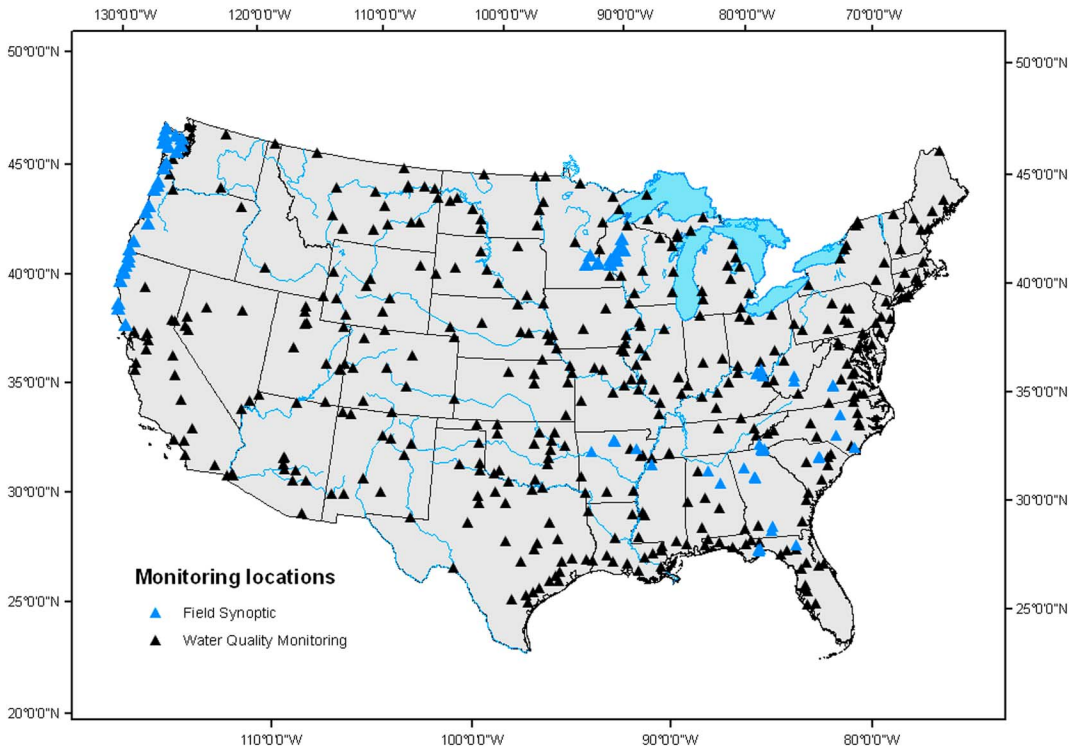

Figure 1. Sampling locations used in this study. The black triangles show locations included for analysis in the water quality monitoring data set. The blue triangles show field synoptic sampling locations.

through the online USGS National Water Information System (https://doi.org/10.5066/F7P55KJN). O_2 concentration data were obtained from National Water Information System (parameter code 00300, in mg O_2 L^{-1}) and converted to μmol L^{-1}. CO_2 and DIC were calculated from reported alkalinity, temperature, and pH (measured via glass electrode) by using the program CO2calc [*Robbins et al*., 2010] using the zero salinity constants [*Millero*, 1979]. *Hunt et al*. [2011] found good agreement between CO_2 calculations by using CO2calc and those made from PHREEQC [*Parkhurst and Appelo*, 1999]. Alkalinity was obtained by selecting among 18 separate parameter codes for either alkalinity, acid neutralizing capacity (i.e., unfiltered alkalinity), or bicarbonate [*Stets et al*., 2014]. In most natural waters, alkalinity is primarily due to weak carbonic acid buffering (HCO_3^-, CO_3^{2-}, and OH^-). However, in low-pH, low-alkalinity systems, organic ligands can contribute to alkalinity and cause erroneously high CO_2 calculation [*Abril et al*., 2015]. To guard against this bias, alkalinity concentrations were corrected for the presence of organic ligands [*Driscoll et al*., 1989]. Paired DOC, alkalinity, and pH data were not ubiquitous in the monitoring data set and hampered the ability to apply consistent corrections for organic ligands at all sites. Because the effect of organic ligands on alkalinity is expected to be most severe in low-alkalinity rivers [*Stets and Striegl*, 2012], the organic ligand correction was only required at monitoring locations with alkalinity <1500 μeq L^{-1}.

Parameter codes 00680 (organic carbon, unfiltered) and 00681 (organic carbon, filtered) were combined and called organic carbon (OC), which should be nearly equivalent to DOC because the particulate portion of organic carbon measured using USGS methods is usually much smaller than the dissolved portion [*Stets and Striegl*, 2012]. OC was used for both the organic ligand correction to alkalinity observations and as a water quality parameter in the subsequent analysis.

Other water quality parameters included the analysis were calcium (parameter code 00915), sulfate (parameter code 00945), and nitrate (parameter codes 00618, 00620, 00630, or 00631).

Water quality data were limited to observations after 1990 because by then most monitoring networks had adopted the incremental end-point titration on filtered water conducted in the field (parameter code 39086), which is considered an extremely robust alkalinity measurement. All observations were required to contain calculated CO_2 and O_2 values. Sites with at least 10 observations after 1990 were included in the analysis,

and the median values of all water quality parameters were used in the analysis. After applying all constraints, approximately 22,000 observations from 339 sites remained in the water quality data set. A flowchart outlining the criteria for data inclusion appears in Figure S2.

2.4. Calculations of Gas Concentrations

The molar deviations of CO_2, O_2, and DIC from atmospheric saturation (ΔCO_2, ΔO_2, and ΔDIC) were calculated on the basis of temperature, barometric pressure (or elevation), assumed atmospheric concentrations of gases, and, in the case of DIC, on measured alkalinity in the sample. The difference between the measured aqueous concentration of a gas (C_W) and its calculated concentration in equilibrium with the atmosphere (C_A) is expressed as $\Delta C = C_W - C_A$. Saturated O_2 concentration (O_{2A}) was calculated from temperature and barometric pressure by using the relationship in *Garcia and Gordon* [1992]. Salinity was assumed to be zero because all observations had specific conductance $<1100\ \mu S\ cm^{-1}$ (not shown). ΔO_2 was then calculated as

$$\Delta O_2 = O_{2W} - O_{2A} \tag{1}$$

where O_{2W} is the measured molar concentration of O_2 in a surface water sample.

CO_{2A} was calculated from an assumed mole fraction of CO_2 in the atmosphere (CO_{2X}) and relating it to a CO_2 concentration in the water by using Henry's law:

$$CO_{2A} = K_H \times CO_{2X} \times P_{ATM} = K_H \times pCO_2 \tag{2}$$

where CO_{2A} is the equilibrium CO_2 concentration ($\mu mol\ L^{-1}$); K_H is the temperature-dependent Henry's constant ($L\ atm\ mol^{-1}$) [*Butler*, 1982]; CO_{2X} is the partial pressure of CO_2 in the atmosphere, assumed to be 390 ppmv; and P_{ATM} is the atmospheric pressure, in atmospheres, calculated from either observed barometric pressure or from the reported elevation of the monitoring location. ΔCO_2 was then calculated as

$$\Delta CO_2 = CO_{2W} - CO_{2A}. \tag{3}$$

ΔDIC was calculated by determining the DIC concentration at atmospheric equilibrium (DIC_A) at a given temperature, pressure, alkalinity, and assumed atmospheric CO_2 mol fraction (CO_{2x} = 390 ppm) and then comparing this with the observed DIC concentration in the sample (DIC_W). ΔDIC differs from ΔCO_2 because the addition or removal of CO_2 is nonlinear due to the ionization of CO_2 to $H^+ + HCO_3^-$ [*Butler*, 1982]. Because of this, CO_2 concentration can be buffered despite large changes in the DIC pool, and the effect is greatest in high-pH, high-alkalinity waters. So ΔDIC is ΔCO_2 plus the ionization products, and therefore, when a water sample is oversaturated in CO_2, $\Delta DIC > \Delta CO_2$, especially in high alkalinity, high-pH systems. Notably, alkalinity is not affected by the ionization/deionization behavior of CO_2 because CO_2 ionization creates both a proton and a bicarbonate ion and so the acid neutralizing capacity of the water remains constant. So

$$\Delta DIC = DIC_W - DIC_A \tag{4}$$

DIC_w was calculated from observed alkalinity, temperature, and pH. DIC_W and DIC_A were calculated by using CO2calc [*Robbins et al.*, 2010].

2.5. Coupled O_2-CO_2-DIC Modeling

The relationships between O_2, CO_2, and DIC are subject to interacting processes of gas exchange, biotic addition or removal of gases, and carbonate buffering. Previous work in oceanic surface waters has shown that temporal lags in CO_2 gas exchange relative to O_2 gas exchange can alter the O_2:CO_2 stoichiometry [*DeGrandpre et al.*, 1998; *Zhai et al.*, 2009]. To better understand the dynamic relationship between O_2, CO_2, and DIC, a coupled model was developed that calculates time series of O_2, CO_2, and DIC by using realistic gas exchange velocity combined with changes in the carbonate system based on CO_2 evasion across the air-water interface. The model uses hypothetical starting concentrations and model conditions to generate time series. The governing equation for oxygen dynamics is

$$O_2(t) = O_2(t-1) + (GPP(t) - ER + k_{O2}[O_2(t-1) - O_{2A}])\Delta t / Z \tag{5}$$

where t is time, Δt is the time interval, Z is water depth in meters, O_2 is the oxygen concentration ($\mu mol\ L^{-1}$), k_{O2} is the O_2 gas exchange velocity ($m\ d^{-1}$), and O_{2A} is the saturated O_2 concentration calculated as in *Garcia*

and Gordon [1992]. GPP and ER are gross primary production and ecosystem respiration, respectively, and are discussed in greater detail below.

DIC dynamics were calculated by accounting for changes in CO_2 concentration resulting from gas exchange and then re-equilibrating the DIC pool at each time step.

$$\mathrm{DIC}(t) = \mathrm{DIC}(t-1) - (\mathrm{GPP}(t) + \mathrm{ER} - k_{CO2}[\mathrm{CO_2}(t-1) - \mathrm{CO_{2A}}])\Delta t / Z \quad (6)$$

where t is time, DIC is the dissolved inorganic carbon concentration ($\mu mol\,L^{-1}$), and k_{CO2} is the CO_2 gas exchange velocity ($m\,d^{-1}$). Initial DIC was an input to the model and then updated at each time step by the processes listed in equation (6). Alkalinity was fixed throughout the model run because addition or removal of CO_2 does not affect alkalinity and the associated changes in alkalinity from nutrient uptake or mineralization were considered to be too small to affect the outcome of the model. $CO_2(t)$ was calculated from DIC(t), alkalinity, and temperature. Mass balances also assume no other DIC or O_2 loss or additions (e.g., from groundwater and calcite formation). Chemically enhanced diffusion of CO_2 was assumed to be minimal because gas exchange velocities were high, which compresses the thickness of the boundary layer and limits the magnitude of CO_2 reaction with OH^-. We tested this assumption by using the equations given in *Wanninkhof and Knox* [1996]. The results showed that chemical enhancement was likely to be less than 15% in this data set, given a k_{CO2} of $4.6\,m\,d^{-1}$ (Table S1 in the supporting information).

Carbonate equilibrium calculations were carried out in PHREEQC [*Parkhurst and Appelo*, 1999]. The model was implemented in R 3.2.3 [*R Core Team*, 2013]. PHREEQC was used because it is a highly flexible equilibrium modeling program that could be integrated into a dynamic model in the R language. Gas exchange was simulated as Fickian diffusion by using assumed gas exchange velocities as part of the input. k_{O2} and k_{CO2} were related by $k_{CO2} = k_{O2} * [Sc_{CO2}/Sc_{O2}]^{-0.67}$, where Sc_{CO2} and Sc_{O2} are the temperature-dependent Schmidt numbers for CO_2 and O_2, respectively [*Wanninkhof*, 1992].

The model was used to demonstrate the coupled behavior of O_2, CO_2, and DIC under several conditions. First, a fixed perturbation from atmospheric equilibrium was allowed to equilibrate over time. Second, simulated time series of O_2, CO_2, and DIC were generated assuming diel changes in the gases due to GPP and ER. Daily sum GPP was held constant, while the GPP at any given time increment, GPP(t), was assumed to be proportional to modeled light.

$$\mathrm{GPP}(t) = I(t) / \Sigma I \quad (7)$$

where GPP is gross primary production ($\mu mol\,O_2\,m^{-2}\,d^{-1}$), $I(t)$ is irradiance at time t, and ΣI is total daily irradiance. I was modeled as in *Yard et al.* [2005], assuming equinox conditions at a stream located at 45°N latitude and 100°W longitude (i.e., 12 h daylight). ER ($\mu mol\,O_2\,m^{-2}\,d^{-1}$) was assumed to remain constant throughout the experiment. Changes in O_2 due to GPP and ER were related to changes in DIC by assuming photosynthetic and respiratory quotients equal to 1. That is, for every mole of O_2 produced, one mole of DIC was consumed and vice versa.

2.6. Statistical Analysis

Parameter distributions in the synoptic field data and the continental-scale water quality monitoring data were non-normal, so nonparametric Spearman correlation was used to describe relationships between water quality variables in the synoptic field data set, as well as in the continental-scale water quality monitoring data set. Statistical descriptions and correlations were performed on individual values in the field data and site medians for the water quality monitoring data. This was done for three reasons: (1) to ensure equal representation of all sites in the water quality monitoring data set, (2) to avoid leverage associated with outliers, and (3) to focus on differences among sites rather than among individual observations. We present a comparison of the results by using all individual observations from the water quality monitoring data set in Table S2. The large number of samples in these data sets increased the likelihood of Type I error, so we interpreted environmental significance of the correlations with consideration of both the statistical significance (P value) and strength of correlation ($|\rho|$).

To describe deviations between ΔO_2 and ΔCO_2, a parameter called excess ΔCO_2, ΔCO_{2EX}, was calculated as $\Delta CO_{2EX} = \Delta CO_2 + \Delta O_2$, where values close to 0 represent observations in which ΔCO_2 and ΔO_2 are close to the

expected stoichiometry based on a predominance of aerobic metabolism. Values >0 suggest that ΔCO_2 exists in excess, and values <0 suggest that ΔCO_2 is less than expected based on ΔO_2. The exact relationship between ΔCO_2 and ΔO_2 will also depend upon assumptions about the respiratory quotient as well as slight differences between k_{O2} and k_{CO2}. In this analysis, respiratory quotient was assumed to be equal to 1.0. The relationship between k_{CO2} and k_{O2} can be expressed as $k_{CO2}/k_{O2} = [Sc_{CO2}/Sc_{O2}]^{-0.67}$ and is 1.05 to 1.10 at most environmental temperatures (not shown). This difference was not considered to be large and so we assumed $k_{O2} = k_{CO2}$ for analysis of the field and water quality monitoring data sets. An analogous parameter expressing the relationship between ΔDIC and ΔO_2, called ΔDIC_{EX}, was also analyzed.

3. Results

3.1. Field Synoptic Measurements

CO_2 was oversaturated in 86 out of 100 observations. pCO_2 ranged from 100 to >14,000 μatm in field samples with mean and median pCO_2 of 2320 and 900 μatm, respectively. Mean and median ΔCO_2 were 61.0 and 20.6 μmol L^{-1}, respectively (Table 1). DIC was oversaturated in 79 out of 99 observations; mean and median ΔDIC were 57.1 and 21.4 μmol L^{-1}, respectively (Table 1). At a small number of sites ($n = 7$), a positive ΔDIC was paired with a negative ΔCO_2, or vice versa. This result is likely due to differences in the way DIC or CO_2 concentration values were obtained by using field methods and calculations. O_2 was undersaturated in 48 out of 101 observations, with mean and median ΔO_2 of −3.3 and −0.2 μmol l^{-1}, respectively (Table 1). Thus, DIC and CO_2 oversaturations were more widespread and larger magnitudes than O_2 undersaturation (Figures 2a and 2b). ΔCO_2 and ΔDIC had significant positive correlations with DOC, iron, and manganese (Table 2). However, the negative correlations with ΔO_2 were strongest relationships in the field synoptic data set (Table 2 and Figures 2a and 2b).

In the water quality monitoring data set, median CO_2 was oversaturated at 319 of 339 monitoring stations. Median pCO_2 at the monitoring stations ranged from 40 to 8200 μatm, and the overall median and mean pCO_2 were 1140 and 1400 μatm, respectively. ΔCO_2 averaged 48.4 μmol L^{-1} with a median of 39.3 μmol L^{-1} (Table 1). DIC was oversaturated at 338 out of 339 monitoring stations, and ΔDIC averaged 95.8 μmol L^{-1} with a median of 82.0 μmol L^{-1} (Table 1). O_2 was undersaturated at 147 out of 339 monitoring locations, and ΔO_2 averaged 13.1 μmol L^{-1} with a median of 6.3 μmol L^{-1} (Table 1). The use of site medians was likely responsible for the small number of sites ($n = 19$) having ΔDIC and ΔCO_2 with opposite signs. As in the field data, CO_2 and DIC oversaturations were larger magnitudes and more common than O_2 undersaturation with 94% and 99% of monitoring stations having positive median ΔCO_2 and ΔDIC, respectively, while 43% of the stations had median $\Delta O_2 < 0$ (Figures 2c and 2d).

In the water quality monitoring data set, ΔCO_2 was positively correlated with organic carbon and nitrate (Table 3). Similar to the field data set, the strongest correlation was with ΔO_2 ($\rho = -0.67$; Table 3 and Figure 2c). ΔDIC was significantly correlated with all parameters analyzed (Table 3). Consideration of both the statistical significance (P value) and strength of correlation ($|\rho|$) shows that the strongest correlations were between ΔDIC and calcium, organic carbon, alkalinity, and ΔO_2 (Table 3). In this case the relationship with ΔO_2 was not the strongest one analyzed (Table 3). Categorizing sites on the basis of alkalinity strengthened the correlations between ΔO_2 and ΔDIC. The correlation between ΔDIC and ΔO_2 among sites with alkalinity <2000 μeq L^{-1} was $\rho = -0.68$ ($P < 0.001$). Among sites with alkalinity >2000 μeq L^{-1} the correlation was $\rho = -0.49$ ($P < 0.001$). Analysis using all of the observations, rather than site medians, showed similar results (Table S2). These results suggest differences in the relationship between ΔDIC and ΔO_2 depending upon alkalinity.

In both the field synoptic and the water quality monitoring data sets, ΔCO_2 and ΔDIC were much larger than ΔO_2 (Figure 2). ΔCO_{2EX} and ΔDIC_{EX} were positive in >85% of all observations in the field and water quality monitoring data sets. Median ΔCO_{2EX} was 32.6 μmol L^{-1} in the field data set and 59.3 μmol L^{-1} in the water quality monitoring data set (Figure 3). Median ΔDIC_{EX} was 34.5 μmol L^{-1} in the field data set and 99.6 μmol L^{-1} in the water quality monitoring data set (Figure 3). In both data sets, ΔCO_{2EX} and ΔDIC_{EX} were larger in rivers and streams with high alkalinity as compared with low alkalinity (Figure 3), although the difference was only moderately significant for ΔCO_{2EX} in the field synoptic data set using Wilcoxon rank-sum correlation (Figure 3).

Table 1. Summary Statistics of Gas Concentrations for the Field Synoptic and Water Quality Monitoring Data Sets[a]

Parameter	Mean ± SD	Median (25th–75th Percentile)	N
Field Synoptic Data Set			
ΔCO2 (μmol L^{-1})	61.0 ± 96.2	20.6 (6.1–56.0)	100
ΔDIC (μmol L^{-1})	57.1 ± 93.3	21.4 (8.1–66.8)	99
ΔO_2 (μmol L^{-1})	−3.3 ± 64.3	−0.2 (−31.1–33.7)	101
Water Quality Monitoring Data Set			
ΔCO_2 (μmol L^{-1})	48.4 ± 41.8	39.3 (22.8–65.7)	339
ΔDIC (μmol L^{-1})	95.8 ± 83.4	82.0 (48.8–121.1)	339
ΔO_2 (μmol L^{-1})	13.1 ± 54.2	6.3 (−20.9–38.8)	339

[a]Mean, median, standard deviation, and 25th–75th percentile ranges are displayed. Statistics for field synoptic data are based on individual observations. Statistics for the water quality monitoring data set were calculated on median values at each monitoring location.

The strength of carbonate buffering is dependent upon pH and alkalinity. Because pH and alkalinity are typically related in freshwaters, the relative importance of carbonate buffering on CO_2 dynamics can be viewed as a function of alkalinity. In relatively low-alkalinity waters (<1000 μeq L^{-1}), ΔCO_2 and ΔDIC are essentially equivalent (Figure 4), suggesting that the pool of ionized CO_2 ($H^+ + HCO_3^-$) is small. However, as alkalinity increases, ΔDIC becomes larger than ΔCO_2, due to the increasing importance of ionized CO_2 (Figure 4). At alkalinity >2000 μeq L^{-1}, the pool of ionized CO_2 is typically larger than the pool of unionized CO_2, not shown. Median alkalinity for the water quality data set was 2780 μeq L^{-1}, suggesting that the effects of carbonate buffering and, particularly, the ionization of CO_2, are important to understanding CO_2 dynamics in a large portion of freshwater systems.

3.2. Coupled Oxygen, Carbon Dioxide, and Dissolved Inorganic Carbon Modeling

The relationship between O_2, CO_2, and DIC was explored in greater detail by using a dynamically coupled model. Inputs to the model are displayed in Table S1. In the first experiment, a water mass enriched in DIC

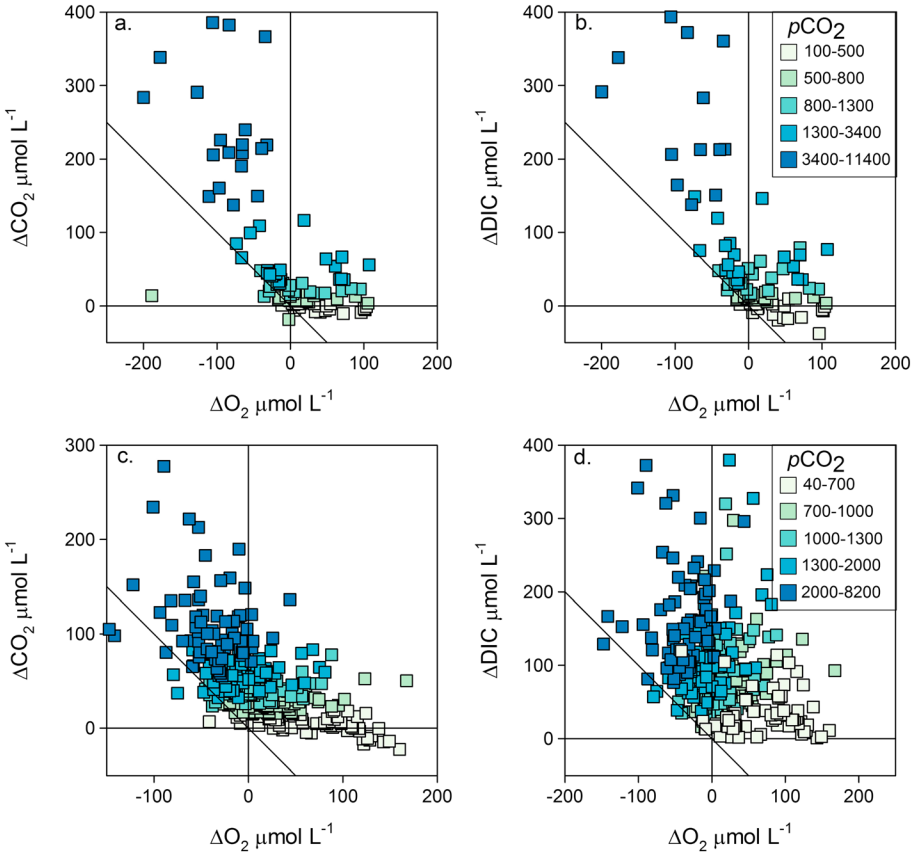

Figure 2. ΔO_2 compared with ΔCO_2 and ΔDIC in the (a and b) field synoptic sampling data set and the (c and d) water quality monitoring data set. Points greater than zero are oversaturated with respect to the atmosphere, and points less than zero are undersaturated. The diagonal line in each figure is the 1:1 line. Points above the line would have ΔCO_{2EX} or ΔDIC_{EX} >0; see text for explanation.

Table 2. ΔCO_2 and ΔDIC Correlations With Water Quality Parameters From the Field Synoptic Sampling Data Set Including Calcium (Ca), Dissolved Organic Carbon (DOC), Iron (Fe), Manganese (Mn), Sulfate (SO_4), Alkalinity, and Oxygen (ΔO_2)[a]

Water Quality Parameter	ΔCO_2	ΔDIC
Calcium ($n = 87$)	−0.02	0.15
Dissolved organic carbon ($n = 96$)	0.33*	0.30*
Iron ($n = 98$)	0.43*	0.34*
Manganese ($n = 98$)	0.52*	0.48*
Sulfate ($n = 87$)	−0.14	−0.15
Alkalinity ($n = 98$)	−0.02	0.07
ΔO_2 ($n = 96$)	−0.63*	−0.62*

[a]The Spearman correlation coefficient is displayed along with the number of observations (n) of each water quality parameter.
*$P < 0.01$.

and depleted in O_2 was allowed to equilibrate passively through gas exchange with the atmosphere. This would be analogous to inputs of groundwater or soil water in a headwater stream. DIC, CO_2, and O_2 dynamics were compared in relatively high- and low-alkalinity waters (2500 versus 1000 $\mu eq\,L^{-1}$, respectively). ΔDIC was initially set to +100 $\mu mol\,L^{-1}$, and ΔO_2 was set to −100 $\mu mol\,L^{-1}$. O_2 equilibrated quickly with the atmosphere such that ΔO_2 was 40 $\mu mol\,L^{-1}$ after approximately 5 h (Figures 5a and 5c). In the low-alkalinity waters, ΔO_2 and ΔDIC converged after approximately 25 h with ΔDIC remaining slightly higher than ΔO_2 for most of the experiment (Figures 5a and 5b). In high-alkalinity waters, DIC lagged behind O_2 equilibration to a much greater degree and remained significantly larger in magnitude than ΔO_2 even after 25 h of equilibration (Figure 5a). ΔDIC is less than $-\Delta O_2$ (i.e., $\Delta DIC_{EX} > 0$) throughout the model run with maximum ΔDIC_{EX} >20 $\mu mol\,L^{-1}$ (Figure 5b). In contrast, ΔCO_2 in both the high- and low-alkalinity scenarios is initially a lower absolute value than ΔO_2 (Figures 5c and 5d), but equilibration proceeds more slowly than O_2 because CO_2 removed through evasion is replaced by CO_2 from the pool of $H^+ + HCO_3^-$ present in the water column. The effect was stronger in the high-alkalinity scenario but was evident whether alkalinity was high or low. Differences in the behavior of ΔDIC and ΔCO_2 result from differences in the direct buffering of CO_2 versus indirect buffering of DIC. In high-alkalinity waters, the equilibration of DIC was greatly affected by buffering of CO_2, which causes some of the CO_2 that could be emitted to the atmosphere to ionize to bicarbonate, thus reducing the gradient of CO_2 across the air-water interface.

The second experiment was meant to simulate diel cycles of O_2, CO_2, and DIC in a moderately productive aquatic ecosystem with negative net ecosystem production (NEP). Daily total gross primary product (GPP) was 4.8 $g\,O_2\,m^{-2}\,d^{-1}$, and ecosystem respiration (ER) was −6.7 $g\,O_2\,m^{-2}\,d^{-1}$, which is similar to the average values for streams reported in *Hoellein et al*. [2013]. The model was applied to waters with high alkalinity (2500 $\mu eq\,L^{-1}$) and low alkalinity (1000 $\mu eq\,L^{-1}$). The model produced diel cycles in O_2, CO_2, and DIC with $\Delta O_2 < 0$ except in the middle part of the light period (Figures 6a and 6b). In low-alkalinity waters, CO_2 and

Table 3. ΔCO_2 and ΔDIC Correlations With Water Quality Parameters From the Water Quality Monitoring Data Set[a]

Water Quality Parameter	ΔCO_2	ΔDIC
Calcium ($n = 335$)	0.06	0.40*
Organic carbon ($n = 187$)	0.45*	0.43*
Nitrate ($n = 338$)	0.37*	0.29*
Sulfate ($n = 335$)	0.09	0.22*
Alkalinity ($n = 339$)	0.09	0.57*
ΔO_2 ($n = 96$)	−0.67*	−0.38*

[a]The analysis includes calcium, organic carbon, nitrate, sulfate, alkalinity, and oxygen (ΔO_2). Correlations were performed on median values for each monitoring location included in the analysis. The Spearman correlation coefficient is displayed along with the number of sites (n) of each water quality parameter.
*$P < 0.01$.

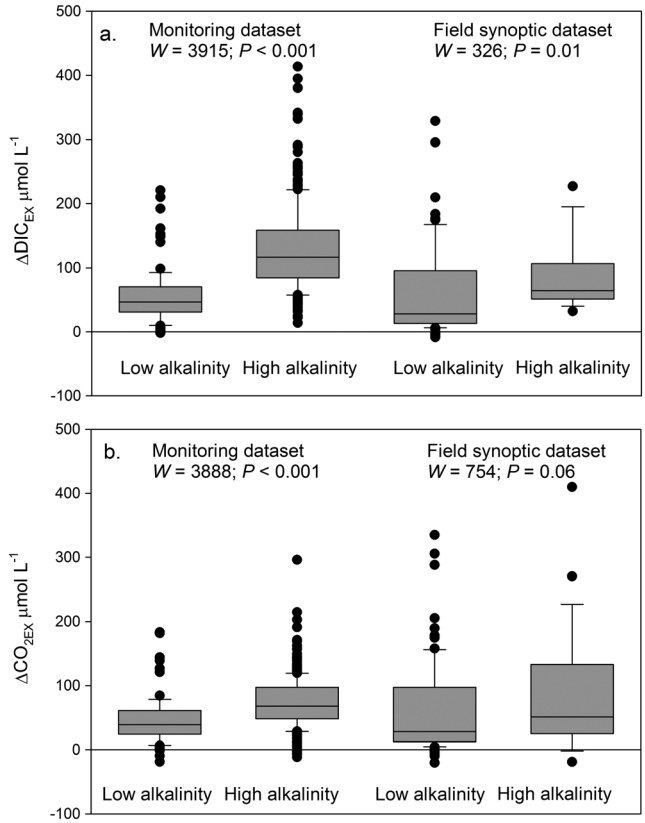

Figure 3. (a) ΔDIC_{EX} and (b) ΔCO_{2EX} from the field synoptic and water quality monitoring data sets. Analyses are divided between high alkalinity ($\geq$2000 µeq L^{-1}) and low alkalinity ($<$2000 µeq L^{-1}). Results of a Wilcoxon signed-rank test (test statistic, *W*, and *P* value, *P*) are displayed on the figure panels.

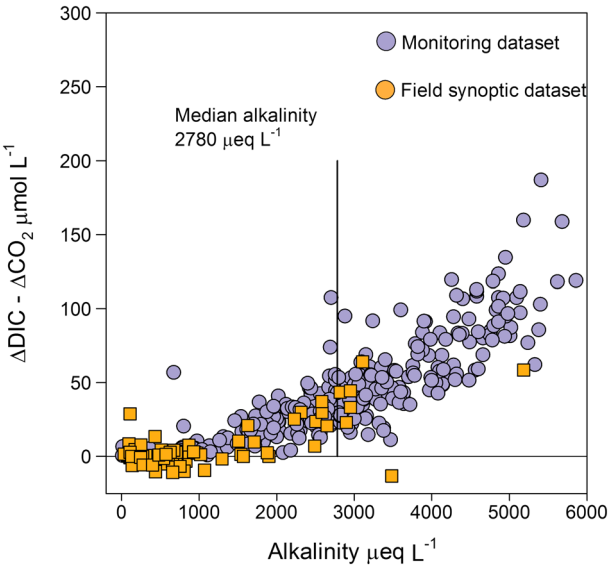

Figure 4. ΔDIC minus ΔCO_2 in the field synoptic (light; orange) and water quality monitoring (dark; purple) data sets plotted against alkalinity. Points above zero indicate that ΔDIC is larger than ΔCO_2. The median alkalinity of all observations is also displayed.

DIC followed similar patterns and became undersaturated in the middle part of the light period (Figure 6a). The similarity in behavior of DIC and CO_2 emphasized that ΔCO_2 and ΔDIC are approximately equivalent in low-alkalinity waters (Figure 4). Nevertheless, the prevalence of data points above the 1:1 line indicates that a discrete sample taken during the day is likely to have ΔCO_{2EX} and/or $\Delta DIC_{EX} > 0$ (Figures 4c and 4e). In high-alkalinity waters, the behavior of CO_2 and DIC differed from each other and from O_2. Both ΔCO_2 and ΔDIC remained >0 throughout the model period, and ΔDIC was substantially larger than ΔCO_2 (Figure 6b).

In the high-alkalinity model system, O_2 oversaturation occurred

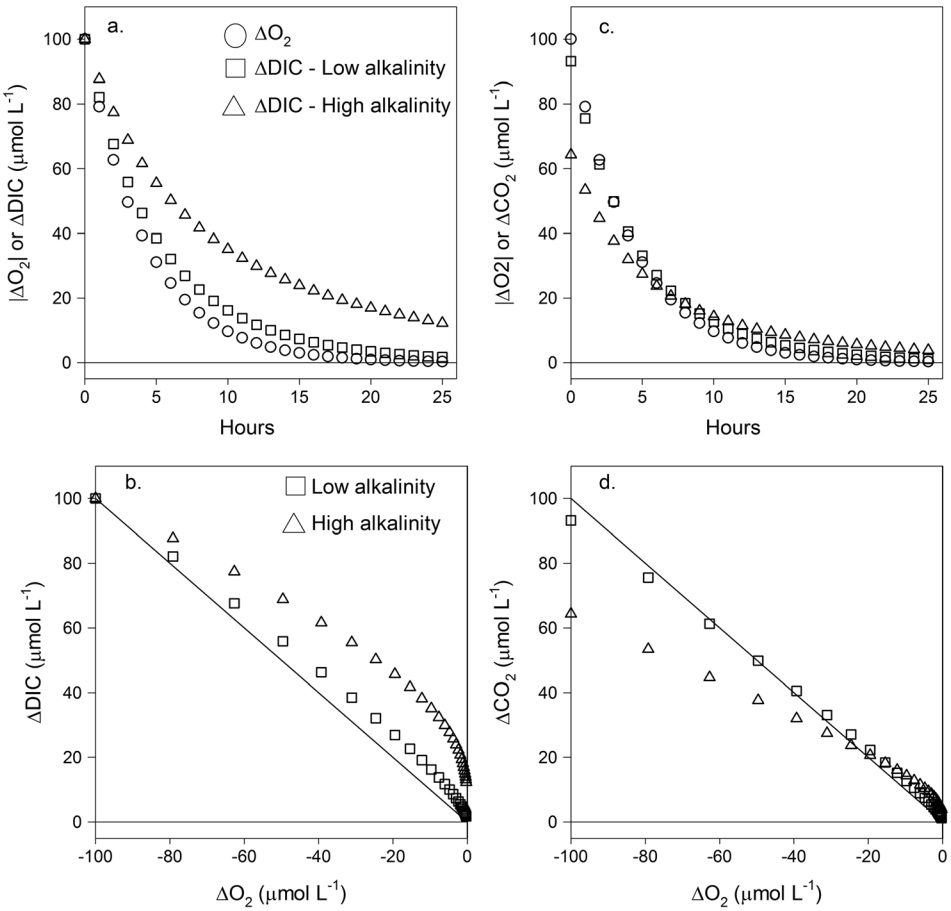

Figure 5. (a) ΔO_2 (circles), ΔDIC in low alkalinity (1000 μeq L^{-1}, squares), and ΔDIC in high alkalinity (2500 μeq L^{-1}, triangles) from the modeling experiment. (b) ΔDIC plotted against ΔO_2 in the low alkalinity (squares) and high alkalinity (triangles) modeling experiments. (c) ΔO_2 (circles), ΔCO_2 in low alkalinity (squares), and ΔDIC in high alkalinity (triangles). (d) ΔCO_2 plotted against ΔO_2 in the low alkalinity (squares) and high alkalinity (triangles). The diagonal line on Figures 5b and 5d is the 1:1 line.

simultaneously with CO_2 and DIC oversaturation for parts of the light period (day) (Figures 6d and 6f). Points above the 1:1 line would produce samples with ΔCO_{2EX} and $\Delta DIC_{EX} > 0$, which was commonly found in the field and water quality monitoring data sets (Figure 3). ΔDIC_{EX} remains positive throughout the model period, whereas ΔCO_{2EX} becomes negative during the night (Figures 6d and 6f). In the low-alkalinity model system, DIC and CO_2 become undersaturated for part of the light period, although samples collected during most of the day would still produce positive ΔDIC_{EX} and ΔCO_{2EX}.

4. Discussion

As expected, ΔO_2 was highly correlated with ΔCO_2 and ΔDIC in both the field and water quality monitoring data sets because of the metabolic linkage between oxygen and carbon (Figure 2). Respiratory or photosynthetic processes in the stream channel and in habitats peripheral to the stream can couple CO_2 and O_2 production or consumption. Chemical oxidation of the end-products of anaerobic metabolism can also consume O_2 and produce CO_2 through acidification, which would also couple O_2 and CO_2 [*Abril et al.*, 2000; *Canfield et al.*, 1993]. The relationship between O_2 and CO_2 or DIC is also consistent with inputs of low-O_2/high-DIC from groundwater or other sources [*Crawford et al.*, 2014; *Richey et al.*, 1988]. Therefore, O_2 consumption broadly encompasses a variety of processes that produce CO_2 (and DIC) and so produces strong correlations at scales ranging from diel patterns at individual sites to continent-wide survey data (Figure 2 [*Borges et al.*, 2015; *Crawford et al.*, 2014]).

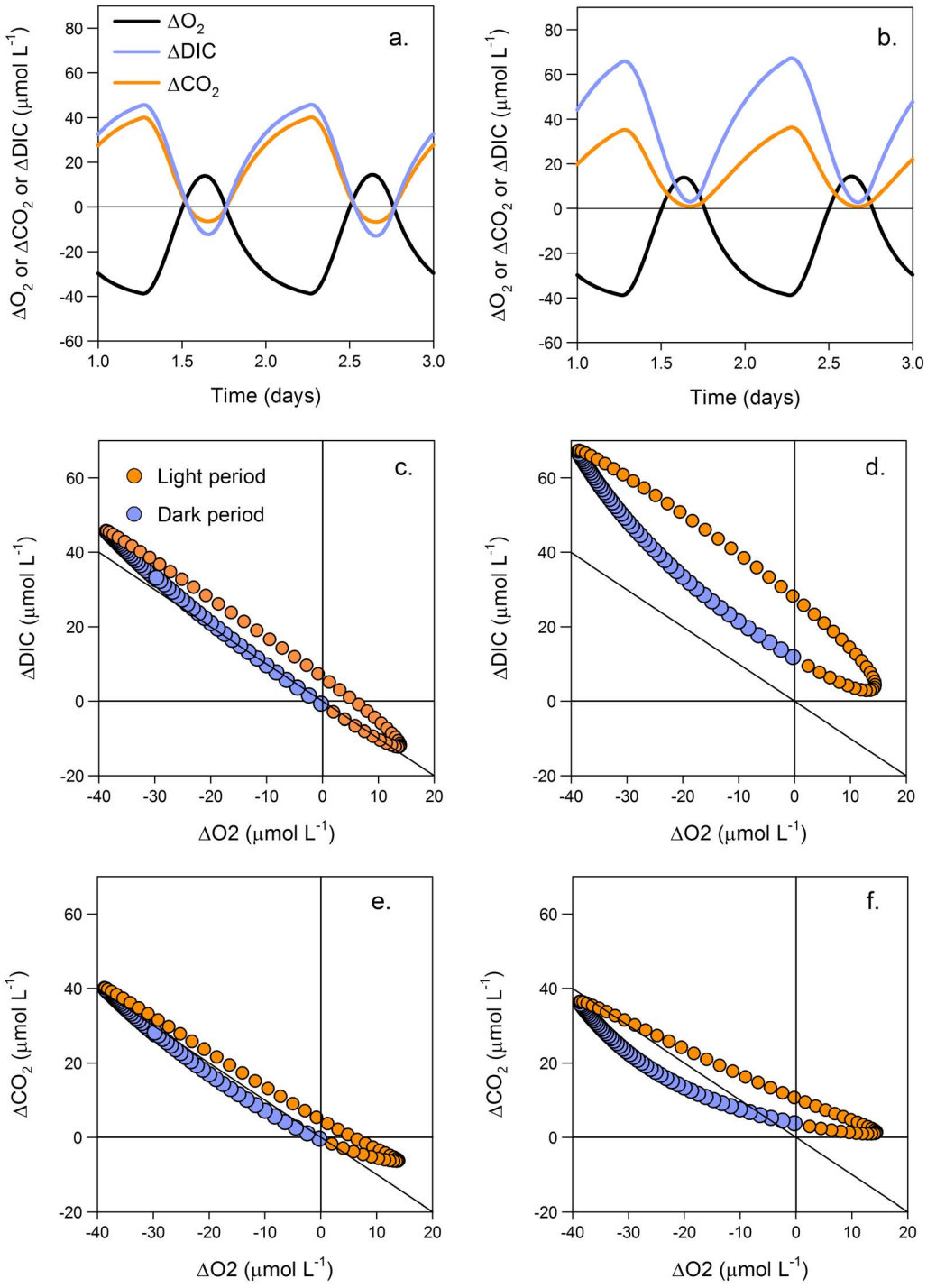

Figure 6. Modeling output time series of ΔO_2 (black line), ΔDIC (purple line), and ΔCO_2 (orange line) in the (a) low alkalinity (1000 μeq L^{-1}) and (b) high alkalinity (2500 μeq L^{-1}) experiments. ΔDIC plotted against ΔO_2 in the (c) low alkalinity and (d) high-alkalinity modeling experiments. The symbol colors denote periods of light (orange, light color) and dark (purple, dark color) in the modeling experiment. The diagonal line is the 1:1 line between ΔO_2 and ΔDIC. Results for ΔCO_2 and ΔO_2 for the (e) low- and (f) high-alkalinity experiments, respectively.

Correlations with other water quality parameters provide important insights into the controls on CO_2 and DIC but explain less of the variability than O_2 concentrations (Tables 2 and 3). The field synoptic and water quality monitoring data sets captured slightly different populations of streams with the field synoptic data set having primarily lower alkalinity (Figure 4) and lower ΔDIC (Table 1). Significantly positive correlations with DOC

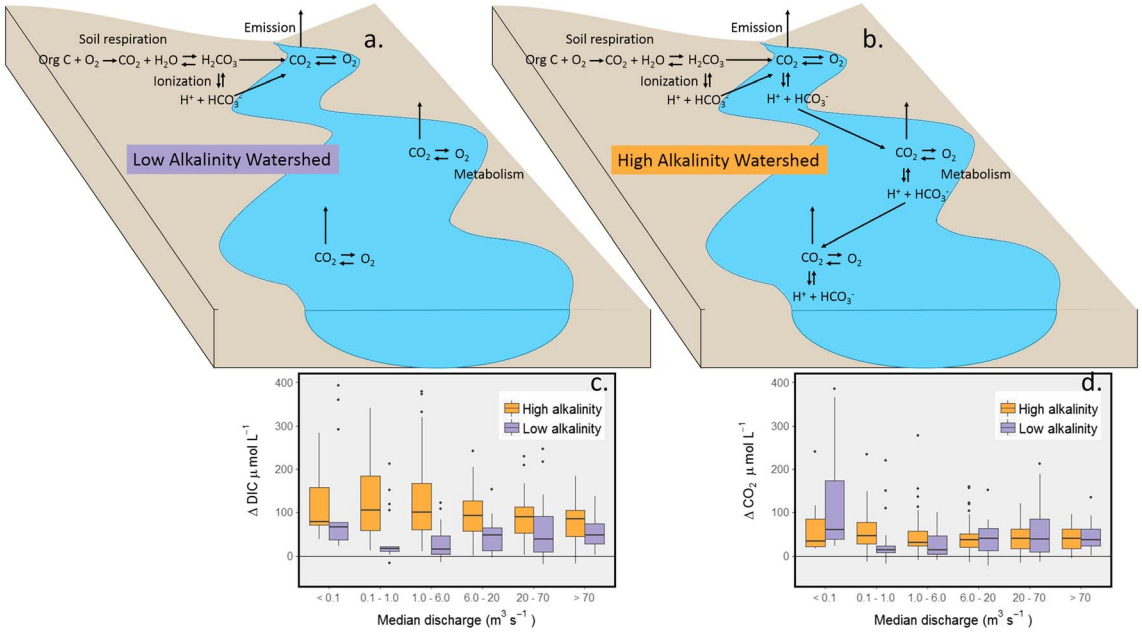

Figure 7. Schematic representing differences in the behavior of CO_2 and DIC in (a) low- and (b) high-alkalinity watersheds. (c) Boxplots of ΔDIC in high alkalinity (≥2000 μeq L^{-1}, orange, light color) and low alkalinity (<2000 μeq L^{-1}, purple, dark color) samples in a gradient of stream size. (d) Similar to Figure 7c but with ΔCO_2 as the response. Boxplots were generated by combining data from the field synoptic and water quality monitoring data sets.

emphasize that reduced organic material is, at the most basic level, the source of CO_2 or DIC oversaturation and that a greater supply of organic material, whether in surface waters, stream hyporheic zones, or soil or groundwater flow paths, leads to higher CO_2 concentrations (Tables 2 and 3). The strong correlations of ΔCO_2 and ΔDIC with iron and manganese in the field data set are also intriguing (Table 2). Iron and manganese were found to be positively correlated with CO_2 evasion in lakes [*Kortelainen et al*., 2013]. Iron concentrations are indicative of the influence of peatlands [*Kortelainen et al*., 2006], and iron can be mobilized under reducing conditions [*Ekström et al*., 2016], suggesting a linkage between stream CO_2 oversaturation and the presence of anoxic environments proximal to the stream channel. However, pH is a major control on iron solubility in soils [*Gotoh and Patrick*, 1974], and so soils with high CO_2 concentrations, and presumably lower pH, would also be expected to have a greater pool of soluble iron. ΔDIC correlations with calcium and alkalinity in the water quality monitoring data set (Table 3) are probably indicative of the influence of carbonate buffering on DIC oversaturation in surface waters.

The carbonate buffering system imparts additional controls on CO_2 concentrations and is closely related to the alkalinity of surface waters (Figure 4). At low alkalinity, ΔCO_2 and ΔDIC are nearly equivalent but diverge at higher alkalinity, emphasizing the importance of ionized forms of CO_2 in high-alkalinity waters (Figure 4). Ionization of CO_2 effectively decreases the gradient of CO_2 across the air-water interface, thereby decreasing CO_2 flux and introducing lags into the CO_2 (or DIC) equilibration times (Figures 5a and 5b). This phenomenon has been described in oceanic systems [*DeGrandpre et al*., 1998; *Zhai et al*., 2009] but has received less attention in freshwaters. Differences in CO_2, DIC, and O_2 dynamics due to carbonate equilibria have been related to the Revelle factor [*Zhai et al*., 2009], which is a function of pH and alkalinity. In our data set, alkalinity ranges from essentially 0 to 5000 μeq L^{-1} with an overall median of 2780 μeq L^{-1}, suggesting that the influence of carbonate equilibria on CO_2 dynamics varies widely but could be important in a large number of streams and rivers.

It is well established that small, low-order streams receive inputs of CO_2 and DIC from groundwater and in-stream negative NEP and that equilibration through atmospheric exchange creates spatial structure in CO_2 oversaturation such that downstream reaches typically have lower CO_2 concentrations [*Finlay*, 2003; *Jones and Mulholland*, 1998]. The rate of equilibration, and therefore the spatial structure of CO_2 oversaturation, depends upon, among other things, the alkalinity of the receiving waters. If the receiving waters have low alkalinity, then most of the incoming ΔDIC would be expressed as CO_2 and equilibrate relatively

rapidly with the atmosphere (Figure 7a). However, in higher alkalinity waters, atmospheric equilibration occurs more slowly because some of the CO_2 delivered to the stream is expressed as $H^+ + HCO_3^-$ and so the gradient of CO_2 across the air-water interface is smaller (Figure 7b). The result of this direct buffering is that CO_2 concentrations in high-alkalinity watersheds remain more constant moving from small upstream waters to downstream rivers. CO_2 buffering also affects the larger DIC pool indirectly, resulting in generally higher ΔDIC in high- versus low-alkalinity watersheds (Figure 7c). As stream size increases, ΔDIC converges in high- and low-alkalinity systems, most likely because the inputs of DIC become smaller and so the effects of carbonate buffering become less apparent (Figure 7c). Likewise, longitudinal patterns in CO_2 differ between high- and low-alkalinity watersheds (Figure 7d). In low-alkalinity streams, CO_2 concentrations are very high in the smallest streams and equilibrate rapidly with the atmosphere resulting in lower CO_2 concentrations in midsize, low-alkalinity streams (median discharge 0.1–6.0 $m^3 s^{-1}$; Figure 7d). In contrast, CO_2 concentrations in the smallest streams of high-alkalinity watersheds (median discharge $< 0.1\ m^3 s^{-1}$) are lower due to CO_2 buffering but remain more consistent moving downstream as CO_2 removed through atmospheric evasion is replaced by equilibration with the ionized forms of CO_2 present in the water column (Figure 7d). CO_2 concentrations are similar in the largest rivers regardless of alkalinity. Therefore, the lags induced by the carbonate buffering system create spatial differences in CO_2 and DIC distributions throughout river networks depending upon the alkalinity of these watersheds.

The approach of considering O_2 and CO_2 simultaneously in surface waters, especially in the context of the full carbonate buffering system, provides important insights into the processes affecting CO_2 oversaturation in these systems. Both data sets that we examined had remarkably similar results using complementary methodology at widely varying spatial and temporal scales. CO_2 dynamics are not fully represented by discrete samples, suggesting that additional information will be gained by observing CO_2 at higher temporal resolution, especially in conjunction with high-frequency O_2 observations. Our analysis provides the most probable mechanism for the imbalanced ΔCO_2:ΔO_2 stoichiometry commonly observed in freshwaters. The other reasons cited for causing ΔCO_2:ΔO_2 stoichiometric imbalances, including anaerobic metabolism, acidification, and rooted plant respiration [*Abril et al*., 2000; *Hamilton et al*., 1995; *Richey et al*., 1988; *Salomão et al*., 2008], have potentially large biogeochemical relevance and may be significant in individual systems. However, we argue that accounting for the influence of the carbonate buffering system on ΔCO_2:ΔO_2 is the primary step needed to improve the general understanding of the CO_2 dynamics for most freshwater ecosystems.

Acknowledgments
We thank Sydney Wilson, Mark Dornblaser, and John Crawford for assisting with the coordination and execution of field work and participating in important discussions on this topic. Two anonymous reviewers helped to improve the manuscript. We also thank the many U.S. Geological Survey personnel who measured streamflow and collected and analyzed water quality samples from the monitoring sites over the years. This work was supported by the USGS LandCarbon Project, the National Research Program, and the USGS Water, Energy, and Biogeochemical Budgets project. Any use of trade, firm, or product names is for descriptive purposes only and does not imply endorsement by the U.S. government. The data used are listed in the references and the U.S. Geological Survey National Water Information System repository at https://doi.org/10.5066/F7P55KJN.

References

Abril, G., H. Etcheber, A. V. Borges, and M. Frankignoulle (2000), Excess atmospheric carbon dioxide transported by rivers into the Scheldt estuary, *C. R. Acad. Sci., Ser. IIA: Earth Planet. Sci.*, *330*(11), 761–768, doi:10.1016/S1251-8050(00)00231-7.

Abril, G., et al. (2015), Technical note: Large overestimation of pCO_2 calculated from pH and alkalinity in acidic, organic-rich freshwaters, *Biogeosciences*, *12*(1), 67–78, doi:10.5194/bg-12-67-2015.

Baker, M. A., C. N. Dahm, and H. M. Valett (1999), Acetate retention and metabolism in the hyporheic zone of a mountain stream, *Limnol. Oceanogr.*, *44*(6), 1530–1539, doi:10.4319/lo.1999.44.6.1530.

Battin, T. J., L. A. Kaplan, S. Findlay, C. S. Hopkinson, E. Marti, A. I. Packman, J. D. Newbold, and F. Sabater (2008), Biophysical controls on organic carbon fluxes in fluvial networks, *Nat. Geosci.*, *1*, 95–100.

Borges, A. V., F. Darchambeau, C. R. Teodoru, T. R. Marwick, F. Tamooh, and N. Geeraert (2015), Globally significant greenhouse-gas emissions from African inland waters, *Nat. Geosci.*, *8*(8), 637–642, doi:10.1038/ngeo2486.

Butler, J. N. (1982), *Carbon Dioxide Equilibria and Their Applications*, Addison-Wesley Publishing Company, Inc., Menlo Park, Calif.

Butman, D., and P. A. Raymond (2011), Significant efflux of carbon dioxide from streams and rivers in the United States, *Nat. Geosci.*, *4*, 839–842, doi:10.1038/ngeo129410.1038/NGEO1294.

Canfield, D. E., B. B. Jørgensen, H. Fossing, R. Glud, J. Gundersen, N. B. Ramsing, B. Thamdrup, J. W. Hansen, L. P. Nielsen, and P. O. J. Hall (1993), Marine sediments, burial, pore water chemistry, microbiology and diagenesis pathways of organic carbon oxidation in three continental margin sediments, *Mar. Geol.*, *113*(1), 27–40, doi:10.1016/0025-3227(93)90147-N.

Crawford, J. T., N. R. Lottig, E. H. Stanley, J. F. Walker, P. C. Hanson, J. C. Finlay, and R. G. Striegl (2014), CO_2 and CH_4 emissions from streams in a lake-rich landscape: Patterns, controls, and regional significance, *Global Biogeochem. Cycles*, *28*, 197–210, doi:10.1002/2013GB004661.

DeGrandpre, M. D., T. R. Hammar, and C. D. Wirick (1998), Short-term pCO_2 and O_2 dynamics in California coastal waters, *Deep Sea Res., Part II*, *45*(8), 1557–1575, doi:10.1016/S0967-0645(98)80006-4.

Driscoll, C. T., R. D. Fuller, and W. D. Schecher (1989), The role of organic acids in the acidification of surface water in the Eastern U.S, *Water Air Soil Pollut.*, *43*, 21–40.

Ekström, S. M., O. Regnell, H. E. Reader, P. A. Nilsson, S. Löfgren, and E. S. Kritzberg (2016), Increasing concentrations of iron in surface waters as a consequence of reducing conditions in the catchment area, *J. Geophys. Res. Biogeosci.*, *121*, 479–493, doi:10.1002/2015JG003141.

Finlay, J. C. (2003), Controls of streamwater dissolved inorganic carbon dynamics in a forested watershed, *Biogeochemistry*, *62*, 231–252.

Garcia, H. E., and L. I. Gordon (1992), Oxygen solubility in seawater: Better fitting equations, *Limnol. Oceanogr.*, *37*(6), 1307–1312, doi:10.4319/lo.1992.37.6.1307.

Gotoh, S., and W. H. Patrick (1974), Transformation of iron in a waterlogged soil as influenced by redox potential and pH1, *Soil Sci. Soc. Am. J.*, *38*(1), 66–71, doi:10.2136/sssaj1974.03615995003800010024x.
Hamilton, S. K., S. J. Sippel, and J. M. Melack (1995), Oxygen depletion and carbon dioxide and methane production in waters of the Pantanal wetland of Brazil, *Biogeochemistry*, *30*(2), 115–141, doi:10.1007/BF00002727.
Hoellein, T. J., D. A. Bruesewitz, and D. C. Richardson (2013), Revisiting Odum (1956): A synthesis of aquatic ecosystem metabolism, *Limnol. Oceanogr.*, *58*(6), 2089–2100, doi:10.4319/lo.203.58.6.2089.
Hotchkiss, E. R., R. O. Hall Jr., R. A. Sponseller, D. Butman, J. Klaminder, H. Laudon, M. Rosvall, and J. Karlsson (2015), Sources of and processes controlling CO_2 emissions change with the size of streams and rivers, *Nat. Geosci.*, *8*(9), 696–699, doi:10.1038/ngeo2507.
Humborg, C., C.-M. Mörth, M. Sundbom, H. Borg, T. Blenckner, R. Giesler, and V. Ittekkot (2010), CO_2 supersaturation along the aquatic conduit in Swedish watersheds as constrained by terrestrial respiration, aquatic respiration and weathering, *Global Change Biol.*, *16*(7), 1966–1978, doi:10.1111/j.1365-2486.2009.02092.x.
Hunt, C. W., J. E. Salisbury, and D. Vandemark (2011), Contribution of non-carbonate anions to river alkalinity and overestimation of pCO_2, *Biogeosci. Discuss.*, *8*(3), 5159–5177, doi:10.5194/bgd-8-5159-2011.
Johnson, M. S., M. F. Billett, K. J. Dinsmore, M. Wallin, K. E. Dyson, and R. S. Jassal (2010), Direct and continuous measurement of dissolved carbon dioxide in freshwater aquatic systems—Method and applications, *Ecohydrology*, *3*(1), 68–78, doi:10.1002/eco.95.
Jones, J., and P. Mulholland (1998), Influence of drainage basin topography and elevation on carbon dioxide and methane supersaturation of stream water, *Biogeochemistry*, *40*(1), 57–72, doi:10.1023/A:1005914121280.
Kempe, S. (1982), Long-term records of CO_2 pressure fluctuations in fresh waters, in *Transport of Carbon and Minerals in Major World Rivers*, *SCOPE/UNEP Sonderb.*, vol. 52, edited by E. T. Degens, pp. 91–332 , Mitt. Geol.-Paläont. Inst. Univ. Hamburg, Hamburg, Germany.
Kortelainen, P., T. Mattsson, L. Finér, M. Ahtiainen, S. Saukkonen, and T. Sallantaus (2006), Controls on the export of C, N, P and Fe from undisturbed boreal catchments, Finland, *Aquat. Sci.*, *68*(4), 453–468, doi:10.1007/s00027-006-0833-6.
Kortelainen, P., M. Rantakari, H. Pajunen, J. T. Huttunen, T. Mattsson, S. Juutinen, T. Larmola, J. Alm, J. Silvola, and P. J. Martikainen (2013), Carbon evasion/accumulation ratio in boreal lakes is linked to nitrogen, *Global Biogeochem. Cycles*, *27*, 363–374, doi:10.1002/gbc.20036.
Lapierre, J.-F., F. Guillemette, M. Berggren, and P. A. del Giorgio (2013), Increases in terrestrially derived carbon stimulate organic carbon processing and CO_2 emissions in boreal aquatic ecosystems, *Nat. Commun.*, *4*, doi:10.1038/ncomms3972.
Laudon, H., M. Berggren, A. Ågren, I. Buffam, K. Bishop, T. Grabs, M. Jansson, and S. Köhler (2011), Patterns and dynamics of dissolved organic carbon (DOC) in boreal streams: The role of processes, connectivity, and scaling, *Ecosystems*, *14*(6), 880–893, doi:10.1007/s10021-011-9452-8.
Marce, R., B. Obrador, J.-A. Morgui, J. Lluis Riera, P. Lopez, and J. Armengol (2015), Carbonate weathering as a driver of CO_2 supersaturation in lakes, *Nat. Geosci.*, *8*(2), 107–111, doi:10.1038/ngeo2341.
McCallister, S. L., and P. A. Del Giorgio (2012), Evidence for the respiration of ancient terrestrial organic C in northern temperate lakes and streams, *Proc. Natl. Acad. Sci. U. S. A.*, *109*(42), 16,963–16,968, doi:10.1073/pnas.1207305109.
McDonald, C. P., E. G. Stets, R. G. Striegl, and D. Butman (2013), Inorganic carbon loading as a primary driver of dissolved carbon dioxide concentrations in the lakes and reservoirs of the contiguous United States, *Global Biogeochem. Cycles*, *27*, 285–295, doi:10.1002/gbc.20032.
Millero, F. J. (1979), The themodynamics of the carbonate system in seawater, *Geochim. Cosmochim. Acta*, *43*(10), 1651–1661, doi:10.1016/0016-7037(79)90184-4.
Oquist, M. G., M. Wallin, J. Seibert, K. Bishop, and H. Laudon (2009), Dissolved inorganic carbon export across the soil/stream interface and its fate in a boreal headwater stream, *Environ. Sci. Technol.*, *43*(19), 7364–7369, doi:10.1021/es900416h.
Parker, S. R., S. R. Poulson, C. H. Gammons, and M. D. DeGrandpre (2005), Biogeochemical controls on diel cycling of stable isotopes of dissolved O_2 and dissolved inorganic carbon in the Big Hole River, Montana, *Environ. Sci. Technol.*, *39*(18), 7134–7140, doi:10.1021/es0505595.
Parkhurst, D. L., and C. A. J. Appelo (1999), User's guide to PHREEQC—A computer program for speciation, batch-reaction, one-dimensional transport, and inverse geochemical calculations, U.S. Geol. Surv. Water Resour. Invest. Rep., 99-4259.
Rantz, S. E., et al. (1982), Measurement and computation of streamflow—Volume 1, Measurement of stage and discharge, and Volume 2, Computation of discharge, U.S. Geol. Surv. Water Supply Pap. 2175. [Available at http://pubs.usgs.gov/wsp/wsp2175/.]
R Core Team (2013), *R: A Language and Environment for Statistical Computing*, R Foundation for Statistical Computing, Vienna, Austria.
Richey, J. E., A. H. Devol, S. C. Wofsy, R. Victoria, and M. N. G. Riberio (1988), Biogenic gases and the oxidation and reduction of carbon in Amazon River and floodplain waters, *Limnol. Oceanogr.*, *33*(4), 551–561, doi:10.4319/lo.1988.33.4.0551.
Robbins, L. L., M. E. Hansen, J. A. Kleypas, and S. C. Meylan (2010), CO2calc—A user-friendly seawater carbon calculator for Windows, Mac OS X, and iOS (iPhone)*Rep.*, U.S. Geol. Surv. Open File Rep., 2010-1280, Reston, Va.
Salomão, M. S. M. B., J. J. Cole, C. A. Clemente, D. M. L. Silva, P. B. de Camargo, R. L. Victoria, and L. A. Martinelli (2008), CO_2 and O_2 dynamics in human-impacted watersheds in the state of São Paulo, Brazil, *Biogeochemistry*, *88*(3), 271–283, doi:10.1007/s10533-008-9210-y.
Schindler, J. E., and D. P. Krabbenhoft (1998), The hyporheic zone as a source of dissolved organic carbon and carbon gases to a temperate forested stream, *Limnol. Oceanogr.*, *43*(2), 157–174.
Stets, E. G., and R. G. Striegl (2012), Carbon export by rivers draining the conterminous United States, *Inland Waters*, *2*(4), 177–184, doi:10.5268/IW-2.4.510.
Stets, E. G., V. J. Kelly, and C. G. Crawford (2014), Long-term trends in alkalinity in large rivers of the conterminous US in relation to acidification, agriculture, and hydrologic modification, *Sci. Total Environ.*, *488–489*, 280–289, doi:10.1016/j.scitotenv.2014.04.054.
Stets, E. G., S. M. Stackpoole, and R. G. Striegl (2015), Synoptic carbon gas fluxes from streams, rivers, and lakes in the conterminous US, USGS Landcarbon, 2012 to 2014, U.S. Geol. Surv. Data Release, doi:10.5066/10.5066/F72B8W2C.
Striegl, R. G., and C. M. Michmerhuizen (1998), Hydrologic influence on methane and carbon dioxide dynamics at two north-central Minnesota lakes, *Limnol. Oceanogr.*, *43*(7), 1519–1529.
Sundquist, E. T., L. N. Plummer, and T. M. L. Wigley (1979), Carbon dioxide in the ocean surface: The homogeneous buffer factor, *Science*, *204*(4398), 1203–1205, doi:10.1126/science.204.4398.1203.
Tobias, C., and J. K. Böhlke (2011), Biological and geochemical controls on diel dissolved inorganic carbon cycling in a low-order agricultural stream: Implications for reach scales and beyond, *Chem. Geol.*, *283*, 18–30, doi:10.1016/j.chemgeo.2010.12.012.
Wanninkhof, R. (1992), Relationship between gas exchange and wind speed over the ocean, *J. Geophys. Res.*, *97*(C5), 7373–7382, doi:10.1029/92JC00188.
Wanninkhof, R., and M. Knox (1996), Chemical enhancement of CO_2 exchanges in natural waters, *Limnol. Oceanogr.*, *41*(4), 689–697.
Yard, M. D., G. E. Bennett, S. N. Mietz, L. G. Coggins Jr., L. E. Stevens, S. Hueftle, and D. W. Blinn (2005), Influence of topographic complexity on solar insolation estimates for the Colorado River, Grand Canyon, AZ, *Ecol. Modell.*, *183*(2–3), 157–172, doi:10.1016/j.ecolmodel.2004.07.027.
Zhai, W., M. Dai, and W.-J. Cai (2009), Coupling of surface pCO_2 and dissolved oxygen in the northern South China Sea: Impacts of contrasting coastal processes, *Biogeosciences*, *6*(11), 2589–2598.